Boyes, R., Slabaugh, G.G. & Beddoe, G. (2009). Fast pseudo-enhancement correction in CT colonography using linear shift-invariant filters. Paper presented at the 16th IEEE International Conference on Image Processing (ICIP), 2009., 07-11-2009 - 10-11-2009, Cairo, Eygpt.

CITY UNIVERSITY LONDON
EST 1894

City Research Online

FAST PSEUDO-ENHANCEMENT CORRECTION IN CT COLONOGRAPHY USING LINEAR SHIFT-INVARIANT FILTERS

Richard Boyes, Greg Slabaugh and Gareth Beddoe

Medicsight PLC, United Kingdom

ABSTRACT

This paper presents a novel method to approximate shift-variant Gaussian filtering of an image using a set of shift-invariant Gaussian filters. This approximation affords filtering of the image using fast convolution techniques that rely on the FFT, while achieving a result that closely matches the shift-variant result. We demonstrate the method in a CT colonography application that reduces the pseudo-enhancement effect, which is a local brightening artifact in CT imaging that can result from the use of oral contrast agents. Experimental results demonstrate the effectiveness of the method and emphasize its computational efficiency.

Index Terms— CT colonography, pseudo-enhancement artifact, shift-variant filtering, shift-invariant filtering

1. INTRODUCTION

1.1. Pseudo Enhancement Effect in CT Colonography

The pseudo enhancement (PEH) effect is a common artifact in computed tomography (CT), manifested as an increased local brightening of darker voxels (corresponding to lower attenuation materials) near brighter voxels (corresponding to higher attenuation materials). This artifact poses problems in CT colonography (CTC), where faecal and fluid residue is typically tagged using an oral contrast agent that has a high attenuation. The contrast agent voxels produce the PEH effect that can alter the true voxel intensities of the structures of interest, namely, colonic polyps. Colonic polyp sizes are important in diagnosis, as those less than a certain size (typically < 10mm) are believed to not be a clinical risk and are thus not surgically removed. Because of the PEH effect, any polyps submerged in the high attenuation tagging fluid may appear to have a decreased size. Furthermore, intensities of polyps or haustral folds may not match that of tissue, leading to problems with electronic removal of the tagging agent. Finally, computer aided detection (CAD) often relies on specific shape and intensity patterns to automatically identify polyps in the scan. If polyps are submerged by tagging agent, these patterns may be altered, leading to reduced detection performance.

Pseudo enhancement primarily results from two factors; beam hardening and x-ray scattering [1]. Beam hardening
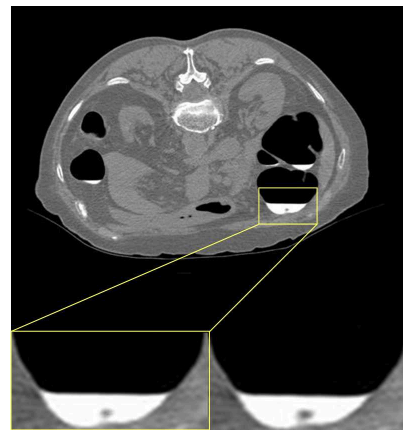
Fig. 1. A CT image with a submerged polyp. Original image (bottom left) and PEH corrected image (bottom right). Note the subtle change in intensity of polyp.

results from the increased attenuation of low energy X-rays compared to high energy X-rays, while scattering, which becomes more dominant as the physical density of the target material increases [2], results from physical interactions of X-rays with the target volume. Typical approaches to correct the pseudo-enhancement effect approximate the PEH as an in-plane (two-dimensional) spatially-variant kernel blurring over high attenuation (intensity) regions [3]. This blurring is then subtracted from the original image, producing a corrected image. In CTC, scans are usually more than 400 512x512 images, and using a shift-variant filter can be prohibitive with regards to computation time. We thus wish to approximate the shift-variant kernel by a sum of *shift-invariant* filters, each of which can be calculated using fast convolution methods, decreasing computation time.

2. LSI APPROXIMATIONS TO SHIFT-VARIANT GAUSSIANS

2.1. Approach

In practice, the PEH is limited to the plane of acquisition (i.e., the image *slice*), primarily due to the spiral CT image acquisition. This simplification means we only need to correct each

image slice in the CT scan. The PEH effect can be modeled using two dimensional shift-variant Gaussian filtering. In particular, each tagged pixel contributes a small amount of its intensity to its neighbors. The shift-variance is present since the variance of the Gaussian is linearly proportional to the image intensity, as depicted in Figure 2. This system can be modeled as a linear shift-variant filter [4] using the equation

$$y[n_1, n_2] = \sum_{k_1} \sum_{k_2} t[k_1, k_2] h_{k_1, k_2}[n_1 - k_1, n_2 - k_2], \quad (1)$$

where $t[n_1, n_2]$ is the tagging image and $h_{k_1, k_2}[n_1 - k_1, n_2 - k_2]$ is a shift-variant isotropic Gaussian filter,

$$h_{k_1, k_2}[k_1, k_2] = \frac{1}{2\pi\sigma^2} e^{-((k_1 - m_1)^2 + (k_2 - m_2)^2)/(2\sigma^2)} \quad (2)$$

centered at the point $[m_1, m_2]$ and having a spatially-varying standard deviation $\sigma[m_1, m_2]$ linearly proportional to $t[m_1, m_2]$. The tagging image $t[n_1, n_2]$ is obtained as

$$t[n_1, n_2] = \begin{cases} x[n_1, n_2] - T, & x[n_1, n_2] > T \\ 0, & \text{otherwise} \end{cases} \quad (3)$$

where $x[n_1, n_2]$ is the original CT image and T is a threshold, typically 100 Hounsfield Units (HU), which represents a cutoff for tagged pixels. We can then subtract Equation 1 from the original image to obtain a PEH corrected image. Assuming the image is of size N x N, and the filter is size M x M, implementing this equation directly requires $O(N^2 M^2)$ operations.
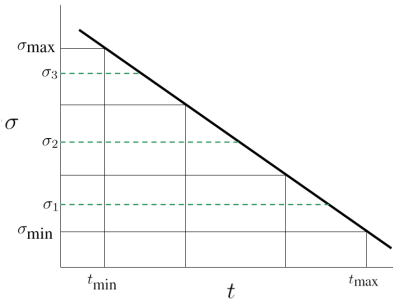
Fig. 2. Estimated standard deviation for a band for a simplified case of $L = 3$ bands.

The shift-variance of this Gaussian filter renders it unsuitable for fast convolution methods that use the FFT. We would like to approximate this linear shift-*variant* filter with using a set of fast linear shift-*invariant* (LSI) filters. To achieve this, we divide the image into L bands based on image intensity, i.e.,

$$t_i[n_1, n_2] = \begin{cases} t[n_1, n_2], & B_i < t[n_1, n_2] <= B_{i+1} \\ 0, & \text{otherwise} \end{cases} \quad (4)$$

where $B_i = t_{\min} + i(t_{\max} - t_{\min})/L$ are intensity thresholds that define the band for $i \in [0 \ldots L]$. For each band,

we determine a corresponding σ_i based on the mean intensity in the band, as depicted in Figure 2. Therefore, each band has an approximating shift-invariant filter $h_i[n_1, n_2] = \frac{1}{2\pi\sigma_i^2} e^{-((n_1 - m_1)^2 + (n_2 - m_2)^2)/(2\sigma_i^2)}$. We can then approximate Equation 1 with a superposition of shift-invariant filterings of the banded images. That is, $y[n_1, n_2] \approx \sum_i t_i[n_1, n_2] * h_i[n_1, n_2]$, where t_i represents the thresholded image for band i, formulated using Equation 4.

In summary, we have approximated the shift-invariant Gaussian filtering of Equation 1 with a superposition of L shift-invariant Gaussian filters. Each 2D shift invariant filter can be computed with computational complexity of $O(LM^2 N \log_2 N)$. However, a further optimization can be realized by implementing the shift invariant Gaussian separably, which reduces the computational complexity to $O(LMN \log_2 N)$. In a practical context, this results in a significant reduction in computation time. The algorithm for the shift-invariant PEH correction is:

1: Initialize pseudo enhancement image $P = 0$
2: L = Number of bands
3: Compute bands $B_i = t_{\min} + i(t_{\max} - t_{\min})/L$
4: **for** $i = 0$ to $L - 1$ **do**
5:     lower = bands(i)
6:     upper = bands($i + 1$)
7:     $\sigma_i = \sigma((\text{lower} + \text{upper})/2)$
8:     Compute linear kernel h_i given σ_i
9:     Compute banded image b_i
10:     Compute thresholded banded image t_i from b_i
11:     Convolve t_i and h_i and add to P
12: **end for**
13: Correct original image by subtracting P

2.2. Analysis

The previous section described our method to approximate the shift-variant filter with a faster shift-invariant filter. One issue not addressed is the impact of the approximation on the accuracy of the results. Approximation of the true Gaussian filter $h_\sigma[k_1, k_2]$ with the banded filter with standard deviation $h_{\sigma_i}[k_1, k_2]$ is bounded by

$$
\begin{aligned}
E &\leq \left[\iint \left(\frac{1}{2\pi\sigma^2} e^{-\frac{1}{2}(x^2 + y^2)/\sigma^2} - \frac{1}{2\pi\sigma_i^2} e^{-\frac{1}{2}(x^2 + y^2)/\sigma_i^2} \right)^2 dx dy \right]^{\frac{1}{2}} \\
&\leq \left[\iint \left(\frac{1}{4\pi^2 \sigma^4} e^{-(x^2 + y^2)/\sigma^2} + \frac{1}{4\pi^2 \sigma_i^4} e^{-(x^2 + y^2)/\sigma_i^2} \right. \right. \\
&\qquad\qquad \left. \left. - \frac{2}{4\pi^2 \sigma^2 \sigma_i^2} e^{-\frac{1}{2}(x^2 + y^2)/\sigma^2} e^{-\frac{1}{2}(x^2 + y^2)/\sigma_i^2} \right)^2 dx dy \right]^{\frac{1}{2}} \\
&\leq \sqrt{\frac{\sigma^4 + \sigma_i^4 - 2\sigma^2 \sigma_i^2}{2\pi\sigma^2 \sigma_i^2 (\sigma^2 + \sigma_i^2)}} \quad (5)
\end{aligned}
$$

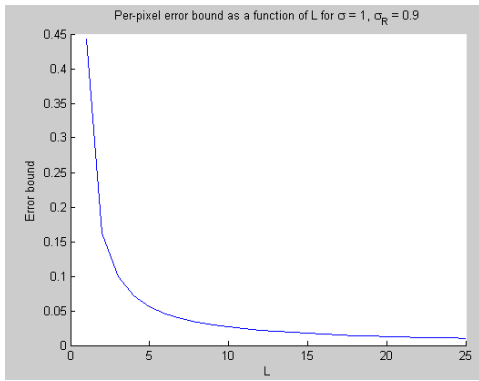As a check, the error goes to zero in the limit as σ_i approaches σ, as expected.

From Figure 2 it is clear that $|\sigma_i - \sigma| \leq \frac{\Delta\sigma}{2}$, where

$$\Delta\sigma = \frac{\sigma_{\max} - \sigma_{\min}}{L} = \frac{\sigma_R}{L} \qquad (6)$$

is the width of a band. Therefore, we can express the bounded error as a function of L as

$$E \leq \sqrt{\frac{\sigma^4 + (\sigma - \frac{\sigma_R}{2L})^4 - 2\sigma^2(\sigma - \frac{\sigma_R}{2L})^2}{2\pi\sigma^2(\sigma - \frac{\sigma_R}{2L})^2(\sigma^2 + (\sigma - \frac{\sigma_R}{2L})^2)}} \qquad (7)$$

An example plot showing the error bound as a function of L is shown in Figure 3. Note that as L increases, the error bound decreases.


Fig. 3. Plot of error bound as a function of L, for $\sigma = 1$, $\sigma_R = 0.9$.
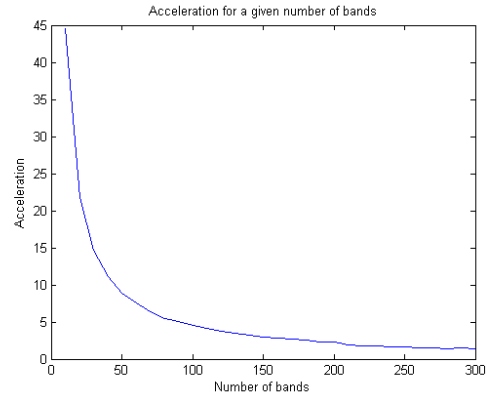
3. EXPERIMENTAL RESULTS

We performed both the shift-variant and shift-invariant approximation filters on a $512\text{x}512$ CT slice, shown in Figure 1, with a significant amount of tagging. In the shift-invariant version of the filter, we varied the number of bands from 10 to 300 between intensities of 100 HU to the image maximum (usually 1000 HU). We then compared the CPU clock time taken for the shift invariant filters to the shift-variant filter, and also calculated the relative intensity error between them over intensities greater than 100 HU i.e., where the filter was applied. Results, shown in Figures 4 and 5, demonstrate that the error, as well as the acceleration are inversely proportional to the number of bands. As an example, with 50 bands, the error is less than 1 percent of the original image intensity but is nearly an order of magnitude faster. In all filters computed, σ was the linear function suggested in [3]: $\sigma = -0.0004x + 0.59$, where x is the image intensity. In all situations a kernel with a half-width of two was used.

In a second experiment, we computed the PEH correction using both the shift-variant and shift-invariant filters for both prone and supine thoracic CT volumes of five different subjects from three separate hospitals, each with residual tagging

agent. In all cases the slice dimensions were $512\text{x}512$. We computed the PEH using the shift-variant filter and invariant filter with 20 bands, and compared the time taken for the two methods for each volume, as well as the error. The results are summarized in Table 1. We typically observed an order of magnitude increase in acceleration using the shift invariant with negligible difference in results. Results can be visually inspected in Figure 6. Note the improved intensities of anatomic structures like polyps and haustral folds.
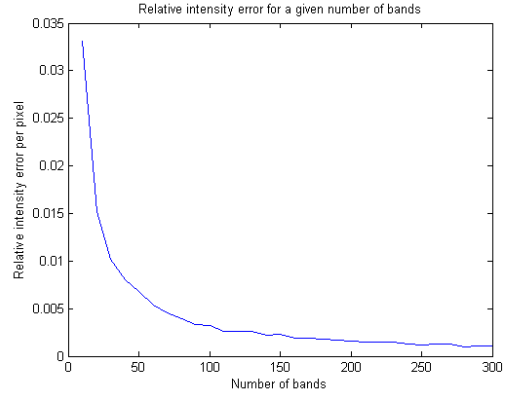

Fig. 4. Experimental result of the the shift-invariant relative error compared to the shift-variant filter for a given number of bands. Compare this experimental error with the theoretical error of Figure 3.

Fig. 5. Experimental result of the acceleration, i.e., the speedup of the shift-invariant filter compared to the shift-variant filter with a given number of bands.

4. CONCLUSION

This paper presented a novel method to approximate a shift-variant Gaussian filter with shift-invariant Gaussian filtering.
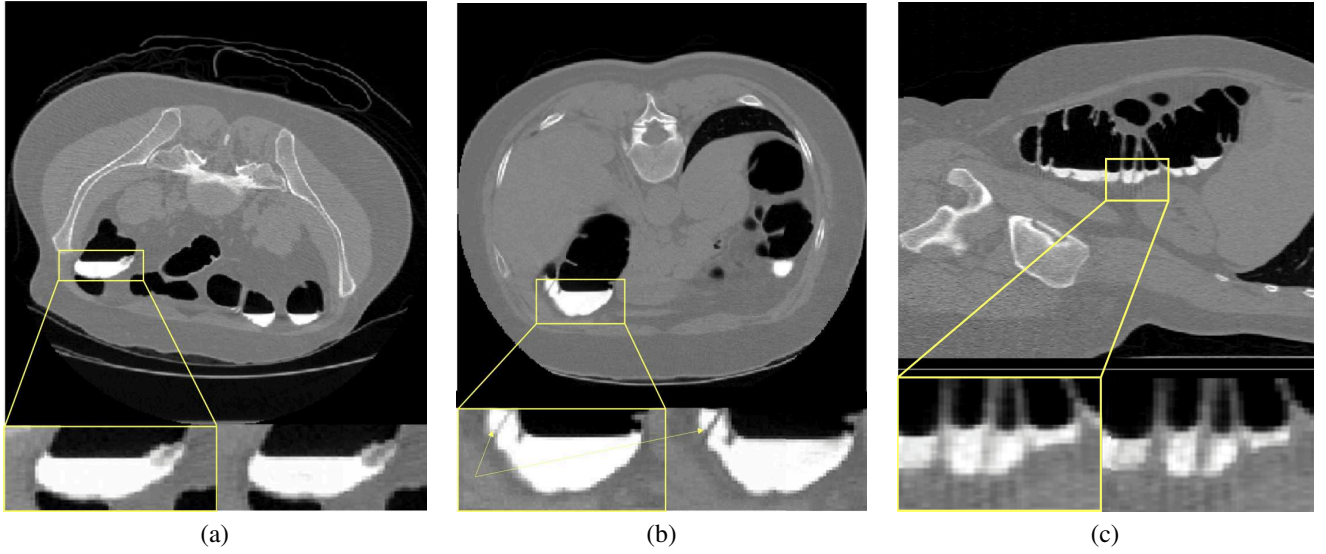
Fig. 6. More results of PEH correction. Improved intensities for a 6mm polyp (a) and haustral folds (b, c). Original images are shown, along with a zoom-in of the original image (lower left) and zoom-in of the corrected image (lower right).

Volume Correction Results					
ID	Orient-ation	#Slices	Relative error	shift-variant time(s)	shift-invariant time(s)
1	Supine	441	0.0104	4000.7	426.0
1	Prone	460	0.0113	4120.6	452.2
2	Supine	444	0.0124	4082.1	428.2
2	Prone	445	0.0096	4028.1	429.8
3	Supine	414	0.0107	3745.8	397.1
3	Prone	423	0.0110	3908.6	406.2
4	Supine	433	0.0093	3980.7	418.1
4	Prone	477	0.0097	4316.8	450.2
5	Supine	443	0.0112	4008.1	422.6
5	Prone	473	0.0108	4296.2	448.7

Table 1. Error and time taken of PEH calculation using both the shift-variant and shift-invariant filters. Note that the time taken includes the disk I/O for each input slice. Acceleration is approximately an order of magnitude.

The approximated algorithm has lower computational complexity, which results in a significant reduction in processing time. We derived an upper bound on the error, which is inversely proportional to the number of bands selected. We demonstrated the method's effectiveness in quickly filtering images for pseudo-enhancement correction, including real CT volumes with residual tagging. In the future, we plan to further study the linear function σ as a function of image intensity. We also plan to extend the method to the case of anisotropic Gaussian filtering, and consider other applications like computing implicit functions as a superposition of radial basis functions [5].

5. REFERENCES

[1] D. Maki, B. Birnbaum, D. Chakraborty, J. Jacobs, B. Carvalho, and G. Herman, "Renal cyst pseudoenhancement: beam hardening effects on ct numbers," *Radiology*, vol. 213, pp. 468 – 472, 1999.

[2] M. Buchmann and D. Mewes, *Optical Measurements: Techniques and Applications*, Springer Verlag, 2001.

[3] J. Nappi and H. Yoshida, "Adaptive correction for the pseudo enhancement of ct attenuation for fecal tagging ct colonography," *Medical Image Analysis*, vol. 12, no. 4, 2008.

[4] A. V. Oppenheim, R. W. Schafer, and J. W. Buck, *Discrete-Time Signal Processing*, Prentice Hall Signal Processing Series, 1998.

[5] H. Q. Dinh, G. Turk, and G. Slabaugh, "Reconstructing surfaces by volumetric regularization using radial basis functions," *IEEE Transactions on Pattern Analysis and Machine Intelligence*, vol. 24, no. 10, pp. 1358 – 1371, 2002.